Collapsing Response of a Nonlinear Shear-Beam Building Model Excited by Horizontal and Vertical Strong-Motion Pulses at Its Base

Hamid Abbasgholiha [1], Vlado Gičev [2], Mihailo D. Trifunac [3], Reza S. Jalali [1] and Maria I. Todorovska [3,4,*]

1 Department of Civil Engineering, Faculty of Engineering, University of Guilan, Rasht P.O. Box 3756, Iran; hamid.abbasgholiha@gmail.com (H.A.); saleh@guilan.ac.ir (R.S.J.)
2 Department of Computer Science, University Goce Delčev, Goce Delčev 89, 2000 Štip, North Macedonia; vlado.gicev@ugd.edu.mk
3 Department of Civil and Environmental Engineering, University of Southern California, Los Angeles, CA 90089-2531, USA; trifunac@usc.edu (M.D.T.); mtodorov@usc.edu (M.I.T.)
4 School of Civil Engineering, Tianjin University, 135 Yaguan Road, Tianjin 300350, China
* Correspondence: mtodorov@tju.edu.cn

Abstract: The sequence of collapsing stages of buildings during strong earthquake shaking is still a poorly understood phenomenon. This study aims to use numerical simulations to improve our understanding of the sequence of phenomena that accompany the collapse of buildings during damaging earthquakes. For that purpose, we use a nonlinear shear-beam model of a building that is excited by a sequence of large horizontal and vertical displacement pulses at its base. The propagation of the input pulses through the structure is simulated by a finite difference scheme. We select the properties of our model to be similar to those of a seven-story hotel in San Fernando Valley of the Los Angeles metropolitan area, which was damaged during the 1994 Northridge, California earthquake. We present results of one example of collapsing response of the model to hypothetical but plausible ground motion close to an earthquake fault. We illustrate the response only for a sequence of horizontal and vertical pulses. We show the differences in the nature of the collapsing sequence for vertical upward and downward pulses of ground motion. Rocking input motions will be added in our future work. Improved understanding of the stages of collapse of buildings will be useful for the development of design strategies to prevent it.

Keywords: building collapse during earthquake; nonlinear shear-beam model; damage in a seven-story hotel; finite difference method

1. Introduction

We present an example of a building model that experiences nonlinear response and collapse when excited at its base by a sequence of *simultaneous* horizontal and vertical displacement pulses. The collapse of a building is a complex physical process, characterized by large material and geometric nonlinearities and interaction between the nonlinear response and the excitation, which develop as the response progresses. To facilitate the understanding and the systematic interpretation of the relative significance of the different components of excitation, we have been investigating this nonlinear problem in stages with progressively increasing complexity of the excitation. In our previous work [1], we considered the same model subjected only to *horizontal* pulse excitation; the study showed that the collapse was initiated by large horizontal deflections, which were consequently taken over by the gravity forces. The vertical inertial forces, caused by the vertical ground motion pulses at the base, introduce dynamic instability and add to the complexity of the response that leads to large nonlinearities and eventually to collapse. Investigation of the role of rocking base motion, acting concurrently with the vertical and horizontal

pulses at the base, is not included in this paper but will be addressed in our future work. Consideration of the effects of soil–structure interaction is also out of the scope of this study.

In this paper, the building model analyzed is a fixed-base shear beam with variable stiffness along its height. We assume that the building has relatively large plan dimensions, compared to the height, in order for it to deform as a whole mostly in shear. The response of the model is computed in the time domain by tracing the propagation of the input displacement pulses using a finite difference scheme. *Collapse in a cell* of the finite difference scheme is defined as the state when its vertical lines reach horizontal position; once this state is reached, it remains unchanged during the subsequent excitation. *Collapse of the structure* is defined as the state in which all cells have collapsed.

Earthquakes, tsunami, hurricanes, explosions, vehicle impact, fires, and terrorist attacks, may cause critical damage to structures that can lead to collapse. Some examples of structural failures that have led to many victims, extensive damage, and social impact include Ronan Point in London, the Capitan Arenas in Barcelona, the Argentine Israelite Mutual Association in Buenos Aires, the Murrah Federal Building in Oklahoma, the Sampoong Department store in Seoul, the World Trade Center in New York, and the Achimota Melcom Shopping Centre in Acra [2]. To prevent such events, structures need to be able to sustain considerable damage without collapsing completely, i.e., to be resilient. Ideally, resilient structures should be able to survive an extreme event and remain functional, as well as to enable restoration to their pre-event performance. Achieving this design goal requires in-depth understanding of the geometry and mechanics of collapse sequences.

Analyses of collapsing structures and proposals for resilient design started to appear around the year 2000. Between 1940, when Lord Baker analyzed buildings damaged by bombs [2], and 2000, there were fewer than five papers per year addressing collapse. By 2010, that number grew to 40 per year, and by 2017 it reached 130 per year [2]. Recent reviews of studies of collapsing behavior of structures appear in Adam et al. [2], El-Towil et al. [3], Byfield et al. [4], Qian and Li [5], and Kunnath et al. [6].

The papers on methods for collapse prevention describe the following three widely used approaches [2]. (1) The *tie force* methods provide the levels of tying, ductility, and continuity required to prevent failure and are recommended for structures with low risk of failure. In buildings, the collapse is initiated when one of its vertical loads carrying members fails, leading to a sequence of failures that can end in total collapse. To prevent these failures, (2) *alternative load path* (ALP) method can be introduced (e.g., Vierendeel action, catenary action, and contribution of the nonstructural elements). When the ALP approach cannot provide sufficient load distribution ability, (3) the *key element* design methods, which introduce key structural elements providing strength of last resort (i.e., structural members, the failure of which initiates the collapse), can be introduced. The ALP method begins with sudden removal of a key load-carrying member and has been used in analyses of modular high-rise buildings [7,8], steel buildings [9], and reinforced concrete (RC) buildings [10,11]. Recorded and observed collapses during demolition of buildings have been used to verify the accuracy of computer simulations [12,13].

The key characteristic of the above proposed methods for prevention of structural failure, leading to collapse, is the educated assumption by the design engineer about which structural members may initiate the failure sequence. Identifying these members is a straightforward decision in the case of placement of explosives for demolition of structures, or when the impact by heavy objects is known in advance. However, these members are impossible to anticipate for shaking by large earthquakes. Observations of failed buildings, following earthquakes, have shown that the failure can be initiated near the top, anywhere along mid-height and at the base of the building. Studies based on wave propagation have shown that this is indeed the case [14–16]. Numerical modeling of buildings that can predict spontaneous initiation of failure, during exposure to strong earthquake shaking, can contribute to our understanding of the sequence of events leading to failure. The numerical model described in this paper can provide this information, in terms of distribution functions describing the outcomes, after it has been shaken by

numerous strong ground motion time histories. Description of the outcomes in terms of distributions is necessary due to the numerous possible outcomes resulting from the mutual interaction of the excitation with the nonlinear response amplitudes.

Evidence of partial and complete collapse of various stone structures, caused by strong earthquakes, could be seen at numerous archeological sites since before the 1900s. In the 1930s, strong motion accelerographs were introduced [17], opening the possibility to record the response of a collapsing building during a strong earthquake, but such response has not yet been recorded. Currently, there are many instrumented structures worldwide; only in a few of them, the response during the early stages of damage has been recorded [18–22].

The approach used in this paper differs from the previous studies in that the collapse begins *spontaneously* with the occurrence of large strains and instabilities caused by the ground motion, and then continues to be governed by the large nonlinear waves and by the action of gravity. Our approach enables studying the locations in the structure at which the collapse is initiated and the factors that influence its initiation, spreading, and the sequence of collapsing displacements.

To the best of our knowledge, there are no instrumented buildings that have experienced collapse during earthquake shaking. In this paper, the parameters of our building model are chosen to correspond approximately to the east-west (EW) response of Van Nuys seven-story hotel (VN7SH; Figure 1), an instrumented reinforced concrete building in the Los Angeles Metropolitan Area, which was lightly damaged by the $M_S = 6.5$ San Fernando earthquake of 9 February 1971, and, 23 years later, severely damaged by the $M_L = 6.4$ Northridge earthquake of 17 January 1994 [18–20]. As a rare example of an instrumented building that has been severely damaged by an earthquake, it has been the subject of or the motivation for many studies [1,14,16,21–31]. During the 1994 Northridge earthquake, its response was recorded by a 13-channel CR-1 central recording system and a self-contained triaxial SMA-1 accelerograph with common trigger time [19,32].
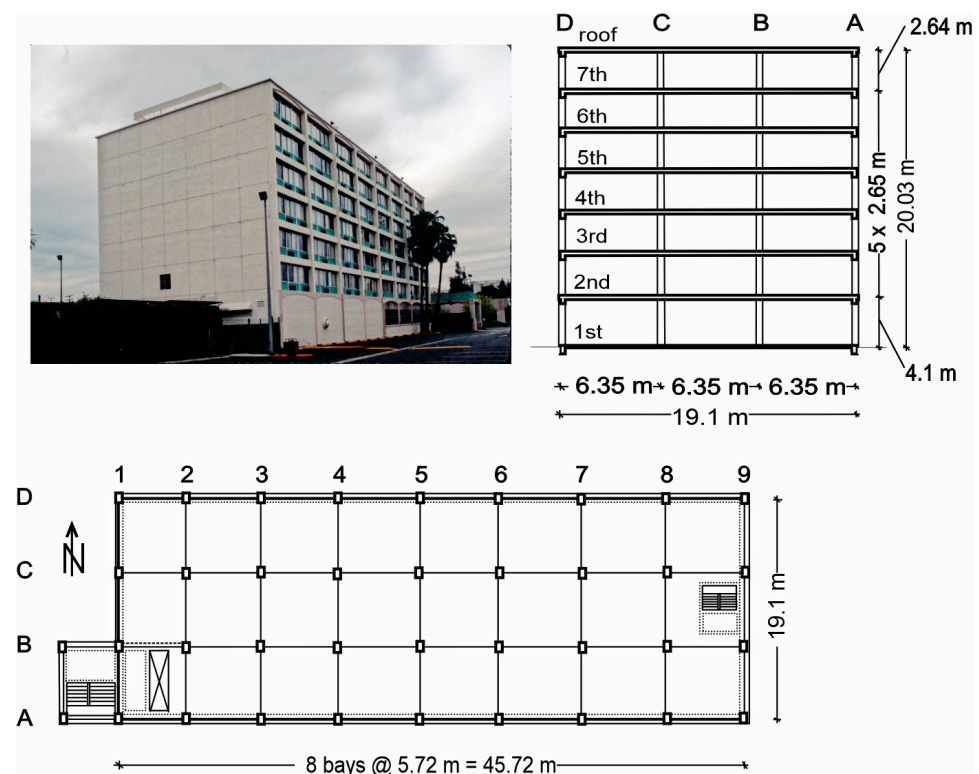

Figure 1. (**Top left**) Northeast view; (**top right**) typical transverse section; and (**bottom**) typical floor framing plan of the Van Nuys seven-story hotel (VN7SH).

The faulting during the San Fernando earthquake of 1971 started at depth of 9 km with a slip of 10 m; its dislocation then spread upward and southwest along approximately a 45° dipping fault, breaking the ground surface at about 12 km northeast of the VN7SH. The vertical surface breaks ranged from 0.5 to 1 m upward and 0.8 to 1.7 m in the strike slip direction [1,33]. During the 1994 Northridge earthquake, the slip was initiated at depth of 17.5 km, about 8 km west of the VN7SH, with a slip of 3 m. The dislocation then propagated up toward northwest and west and stopped at depth of 5 km below the ground surface. The fault was 18 km long and 24 km wide [1,34].

Detailed description of the building and of the damage caused by the Northridge earthquake can be found in [18–20]; a recent summary can be found in [1]. Herein, we include only a brief description of the structure and a review of the damage. Figure 1 shows a photo of the building, a typical transverse section, and a typical floor plan, in which the column lines have been marked and the dimensions of the structure have been specified. Figure 2a shows the shear-beam model and the distribution of the shear-wave velocity along its height (discussed in more detail in the next section), and Figure 2b shows a photo of the north side of the building and views of columns A7 and A8, which were severely damaged. The structural damage was most severe in the exterior north (D) and south (A) frames, which had been designed to resist most of the lateral loads in the longitudinal (EW) direction (Figure 1). Below the 5th floor, shear cracks occurred in the columns of frame A, near the contact with the spandrel beam (Figure 2b) [1]. The shear cracks in the north (D) frame were minor. There was no damage to the interior longitudinal (B and C) frames, and there was no visible damage to the slabs or around the foundation. The nonstructural damage was significant.
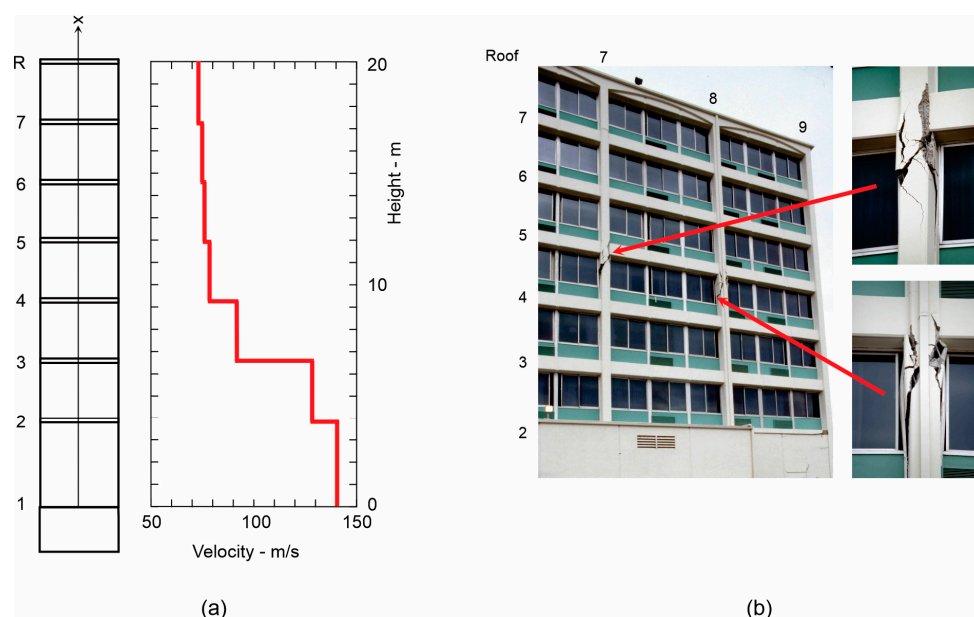

Figure 2. (**a**) The model (layered shear beam) and its shear-wave velocity profile, based on ambient vibration tests [23]. (**b**) View of columns A7 and A8, which were severely damaged by the 1994 Northridge earthquake (located on the north side of the VN7SH building).

The response of the building to the Northridge earthquake was recorded at the ground, second, third, and sixth floors, and at the roof. Figure 3a shows the first 25 s of the east-west (EW) displacements. The five highlighted peaks in the recorded ground displacement, all acting in the same direction, are used in this paper as a guide in adopting simplified excitation by a sequence of five half-sine pulses. Figure 3a, shows one pulse with amplitude A and duration t_d. The response of the model was computed for several cases of a sequence of pulses, which are shown in the figures presenting the results. The amplitudes of the pulses are hypothetical and are meant to illustrate only one possible path toward complete

collapse of the model. We will consider various combinations of pulses, differing in their total number, relative amplitudes, directions of action and duration, in our future generalizations of this work and associated sensitivity studies.
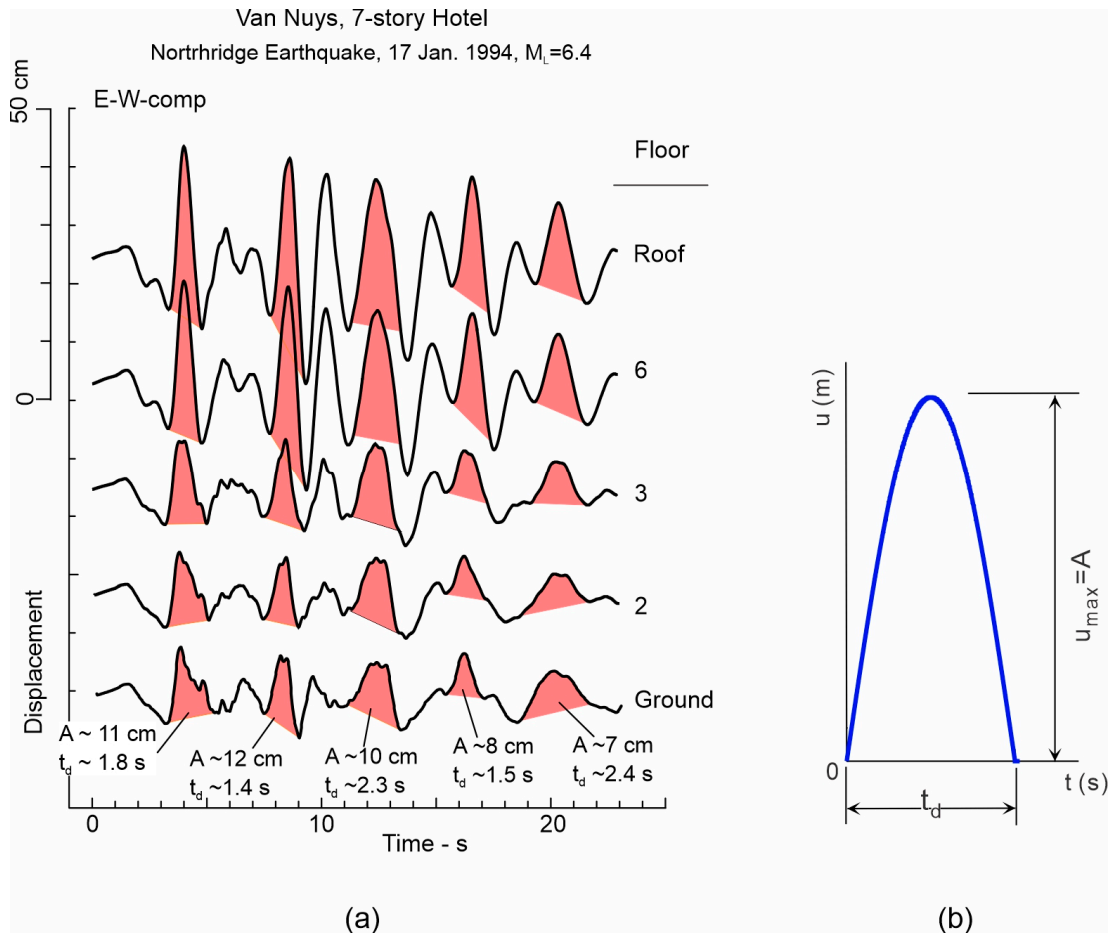

Figure 3. (**a**) The first 25 s of the EW component of displacement, recorded in VN7SH building during the 1994 Northridge earthquake, at ground level, second, third, and sixth floors, and at the roof. Pulses in the displacement responses are emphasized by shades. At ground level, the pulses have amplitudes $A \sim$11, 12, 10, 8, and 7 cm, durations $t_d = 1.8$, 1.4, 2.3, 1.5, and 2.4 s, and occur at time $t = 3.1$, 7.8, 11.2, 15.6, and 19.1 s after trigger. (**b**) Model of an input horizontal ground motion pulse. The vertical pulse of the same shape will have amplitudes 1/5, 1/2, 3/4 of A.

This paper is organized as follows. The Materials and Methods section present the model and the method of solution. The method is the same as in [1]; only a summary is presented in this paper for the purpose of completeness. The Results section presents plots of the model displacements at various moments of time until collapse occurs, and the Discussion and Conclusions section presents the conclusions of this study.

2. Materials and Methods

2.1. Model

The one-dimensional (1D) structural model is a fixed-base shear beam of height H_b and with piecewise constant varying stiffness, determined from ambient vibration tests of the VN7SH (Figure 2a) [25]. Since the measurements could not resolve the stiffness associated with the individual structural members, the floor slabs were not modeled explicitly. Every floor of the building is represented as a layer, with height h_i, mass density ρ_i, and shear-wave velocity β_i, $i = 1$ to 7. The numerical values of these parameters are shown in Table 1 and the wave velocity profile is shown next to the building model in

Figure 2a. Overall, the total height $H_b = 20.036$ m and the average shear-wave velocity is $\beta_b = H_b / \sum_{i=1}^{7} \frac{h_i}{\beta_i} = 91.79$ m/s.

Table 1. One-dimensional VN7SH model assumed to be fixed at its base.

Story	Story Height (m) h_i	Number of Spatial Intervals in Each Story	β_i (m/s)	ρ_i (kg/m^3)
1	3.987	59	140.20	76.92
2	2.675	39	129.50	82.90
3	2.656	39	91.44	82.90
4	2.656	39	79.25	82.90
5	2.656	39	77.72	82.90
5	2.6555	39	76.20	82.90
7	2.7505	40	73.15	82.90

The motion of the model is described in the $x - O - y$, which has origin at the base, as shown in Figure 2a. Its horizontal and vertical displacements $u(t)$ and $v(t)$ are positive, respectively in the positive $x-$ and $y-$ directions. The structure is excited by horizontal and vertical displacements at the base u_g and v_g.

The finite difference model of the building is divided into 294 spatial intervals in such a way that point N on the top of the building is the 295th point of the model (Figure 4a). In order to simplify the computation of the spatial derivative in the numerical calculations, a dummy point N' is defined as the 296th point of the model, at distance dy above the top point N.
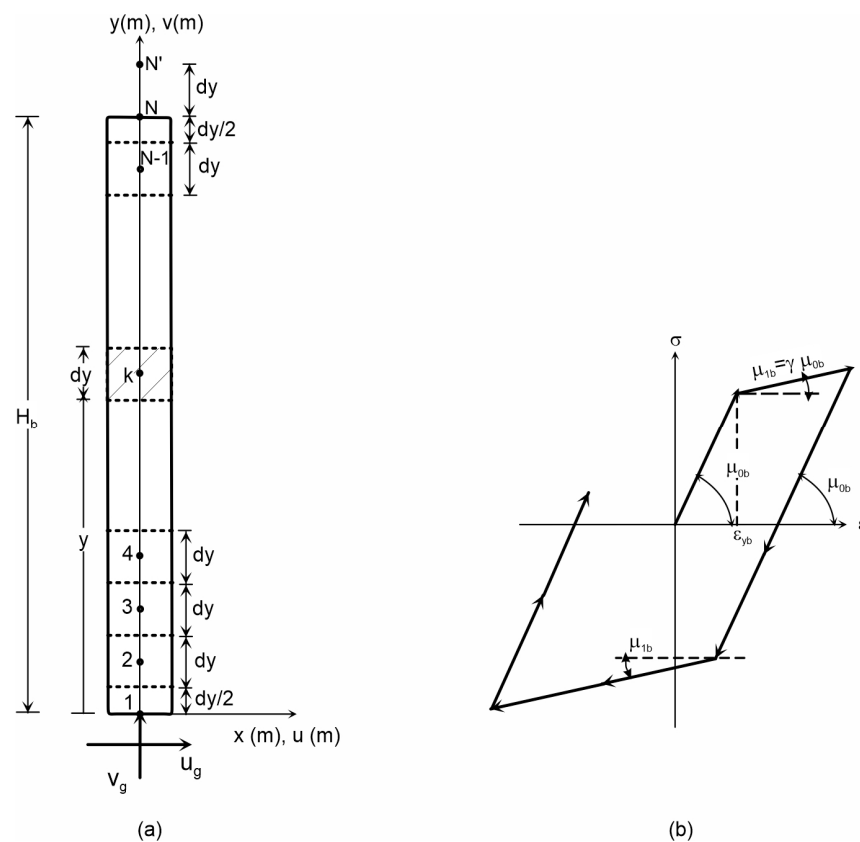

Figure 4. (**a**) The model: Shear building with fixed base. (**b**) The constitutive law for the shear building material.

A bilinear stress–strain relationship $\sigma = \sigma(\varepsilon)$ is adopted for the material such that the ratio between the second and the first slopes $\gamma = 0.44$; the maximum linear strain is selected as $\varepsilon_{yb} = 0.0025$ (Figure 4b). This stress–strain relationship has been selected based on several response analyses using simplified engineering push-over methods, reviewed, interpreted, and then adopted as in [14].

The finite difference scheme propagates the wave motion into the model. This motion is initiated with horizontal and vertical pulses at the base, upward into the model. The wave propagates into the beam with local linear velocity, defined in Figure 2a, when the amplitudes are in the linear range, and with reduced velocities (Figure 4b) when the strains exceed ε_{yb}. For long waves, the finite difference scheme combines the wave motion propagating from the base upward with the wave motion reflected from the top of the beam and propagating downward.

2.2. Equations of Motion and Compatibility Conditions

Figure 5a shows a free-body diagram of an arbitrary element k of the beam at the n-th time step. The element has length dy and cross-sectional area $A' = \Delta x\ \Delta z = 1$. The absolute horizontal and vertical displacements of its center are u and v. At time t, it undergoes rotation ε_k and is subjected to inertia body forces $\rho \ddot{u}$ and $\rho \ddot{v}$, self-weight ρg, per unit volume, and to shear and normal stresses $\tau_{\xi\eta}$ and σ_y, acting on the cross-sectional area of the deformed element. The local coordinate ξ has origin at the center of the element and is oriented in its longitudinal direction, while the local coordinate η is eliminated since the model is 1D (Figure 5a). Upon coordinate transformation from the $x - y$ to the $\xi - \eta$ coordinate system, the dynamic equilibrium equations in the horizontal and vertical directions become as follows [1]:

$$\frac{\partial v_x}{\partial t} = \frac{1}{\rho \cos^2 \varepsilon_k} \frac{\partial \tau_{\xi,\eta}}{\partial y} \tag{1}$$

$$\frac{\partial v_y}{\partial t} = \frac{1}{\rho \cos^2 \varepsilon_k} \frac{\partial \sigma_y}{\partial y} - g \tag{2}$$
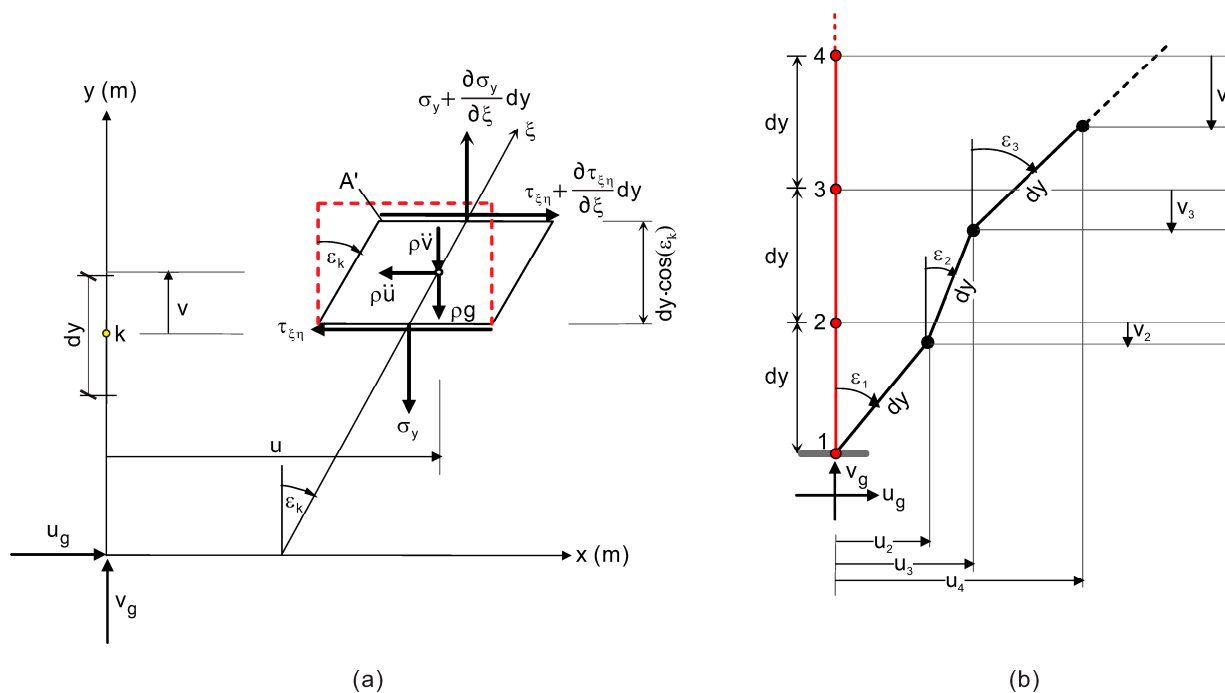

(a)　　　　　　　　　　　　　　　　　　　　　　　　　　　　　　　(b)

Figure 5. (**a**) Free body diagram of element k (**b**) Horizontal and vertical displacements and rotations of the model.

To obtain the compatibility equation that relates the horizontal and vertical velocities at the center of elements k and $k + 1$, a *connecting element k*, between these points is introduced, in order that it has length dy and moves by rotation ε_k and angular velocity ω (Figure 5b). The angular velocity is positive counterclockwise while the rotation of the connecting element and its time derivative $\dot{\varepsilon}_k$ are positive clockwise. Based on the principles of kinematics of rigid bodies, the horizontal and vertical velocities of points k and $k + 1$ are related to each other by the compatibility equation for the connecting element k [1]:

$$\dot{\varepsilon}_k = \frac{\partial v_x}{\partial y} \cos \varepsilon_k - \frac{\partial v_y}{\partial y} \sin \varepsilon_k \tag{3}$$

2.3. The Finite Difference Scheme

The set of simultaneous equations is solved by the Lax and Wendroff's $O(dt^2, dy^2)$ finite difference scheme [35]. For this purpose, a matrix form of Equations (1)–(3) is defined as

$$[\mathbf{U},_t]_{3\times1} = [\mathbf{B}]_{3\times2}[\mathbf{F},_y]_{2\times1} + [\mathbf{G}]_{3\times1} \tag{4}$$

in which

$$
\mathbf{U} = \left\{ \begin{array}{c} v_x \\ v_y \\ \varepsilon_k \end{array} \right\}, \ \mathbf{F} = \left\{ \begin{array}{c} \tau_{\xi\eta} \\ \sigma_y \end{array} \right\}, \ \mathbf{G} = \left\{ \begin{array}{c} 0 \\ -g \\ \frac{\partial v_x}{\partial y} \cos \varepsilon_k - \frac{\partial v_y}{\partial y} \sin \varepsilon_k \end{array} \right\},
$$

$$
\mathbf{B} = \left[\begin{array}{cc} \frac{1}{\rho \, \cos^2 \varepsilon_k} & 0 \\ 0 & \frac{1}{\rho \, \cos^2 \varepsilon_k} \\ 0 & 0 \end{array} \right]
\tag{5}
$$

Upon expanding $\mathbf{U}$ in Taylor series up to the third term and introducing Jacobian matrix for vectors $\mathbf{U}$ and $\mathbf{F}$ ([1]), vector $\mathbf{U}$ at time step $n + 1$, and in the center of element k is computed as

$$\mathbf{U}_{k,n+1} = \mathbf{U}_{k,n} + \frac{\Delta t}{\rho}\mathbf{C}_{k,n} + \frac{\Delta t^2}{2\rho}\mathbf{D}_{k,n} + \frac{\Delta t^2}{2\rho}\mathbf{E}_{k,n} \tag{6}$$

in which

$$
\mathbf{C}_{k,n} = \left\{ \begin{array}{c} \frac{1}{\cos^2 \varepsilon_k} \frac{\partial \tau_{\xi\eta}}{\partial y} \\ \frac{1}{\cos^2 \varepsilon_k} \frac{\partial \sigma_y}{\partial y} - \rho g \\ \rho \left(\frac{\partial v_x}{\partial y} \cos \varepsilon_k - \frac{\partial v_y}{\partial y} \sin \varepsilon_k \right) \end{array} \right\}_{k,n}
\tag{7}
$$

$$
\mathbf{D}_{k,n} = \left\{ \begin{array}{c} \frac{1}{\cos^4 \varepsilon_k}\left[\sin(2\varepsilon_k)\left(\frac{\partial v_x}{\partial y} \cos \varepsilon_k - \frac{\partial v_y}{\partial y} \sin \varepsilon_k \right) \right]\left(\frac{\partial \tau_{\xi\eta}}{\partial y} \right) \\ \frac{1}{\cos^4 \varepsilon_k}\left[\sin(2\varepsilon_k)\left(\frac{\partial v_x}{\partial y} \cos \varepsilon_k - \frac{\partial v_y}{\partial y} \sin \varepsilon_k \right)\left(\frac{\partial \sigma_y}{\partial y} \right) \right] \\ \frac{\partial}{\partial y}\left(\frac{1}{\cos^2 \varepsilon_k} \frac{\partial \tau_{\xi\eta}}{\partial y} \right)\cos \varepsilon_k - \frac{\partial}{\partial y}\left(\frac{1}{\cos^2 \varepsilon_k} \frac{\partial \sigma_y}{\partial y} \right)\sin \varepsilon_k + \\ +\rho\left\{ -\frac{\partial v_x}{\partial y}\frac{\partial v_y}{\partial y}\cos(2\varepsilon_k) - \frac{1}{2}\left[\left(\frac{\partial v_x}{\partial y} \right)^2 - \left(\frac{\partial v_y}{\partial y} \right)^2 \right]\sin(2\varepsilon_k) \right\} \end{array} \right\}_{k,n}
\tag{8}
$$

$$
\mathbf{E}_{k,n} = \left\{ \begin{array}{c} \frac{1}{\cos^2 \varepsilon_k}\frac{\partial}{\partial y}\left[\left(\frac{\partial v_x}{\partial y} \cos \varepsilon_k - \frac{\partial v_y}{\partial y} \sin \varepsilon_k \right)\frac{\partial \tau_{\xi\eta}}{\partial \varepsilon} \right] \\ \frac{1}{\cos^2 \varepsilon_k}\frac{\partial}{\partial y}\left[\left(\frac{\partial v_x}{\partial y} \cos \varepsilon_k - \frac{\partial v_y}{\partial y} \sin \varepsilon_k \right)\frac{\partial \sigma_y}{\partial \varepsilon} \right] \\ 0 \end{array} \right\}_{k,n}
\tag{9}
$$

2.4. Stresses, Boundary Conditions, and Displacements

The normal stress σ_y at the center of element k and at time step n is computed using the rotation ε and the vertical acceleration $\ddot{v}$ of the center of the elements above it [1]. To

satisfy the stress-free boundary condition at the top (point 295 in Figure 4a) at all times, the horizontal and vertical velocities and the derivatives of the shear and normal stresses, with respect to the shear strain or rotation $\frac{\partial \tau_{\xi\eta}}{\partial \varepsilon}$ and $\frac{\partial \sigma_y}{\partial \varepsilon}$ at the dummy point (point 296 in Figure 4a) should be the negative of the corresponding values at point 294. Moreover, the shear and normal stresses at point 296 should be the same as the corresponding values at point 294 [1]. The geometric definition of horizontal and vertical positions and rotations of the first and other connecting elements are shown in Figure 5b.

The horizontal and vertical positions of the center of element k at time step n, $X_{k,n}$, and $Y_{k,n}$ are computed using the rotations of the element below it. Suppose $\varepsilon_{k,n}$ is the rotation of the element connecting the centers of elements k and $k + 1$ at time step n. Then,

$$X_{k,n} = (U_g)_{1,n} + \sum_{j=1}^{k-1} \sin \varepsilon_{j,n} dy \tag{10}$$

$$Y_{k,n} = (V_g)_{1,n} + \sum_{j=1}^{k-1} \cos \varepsilon_{j,n} dy \tag{11}$$

2.5. Definition of Collapse

The collapse of a layer, which has height dy, occurs when its vertical lines rotate by an angle of $\pm\pi/2$ and become horizontal. Once this occurs, the layer is not allowed to deform any further and its rotation is set permanently to $\pm\pi/2$. This shifts the vertical axis of the model by $\pm dy/2$ at this layer and everywhere above it, which increases the overturning moment and contributes to the collapse of the adjacent elements above and below it.

3. Results

We use the observed damage in VN7SH as a qualitative guide to define cases that would be interesting to investigate. We do not attempt to model its response realistically and in detail since we would need accurate modeling of the building, which, in turn, would lead to complexities in the results, making it difficult to interpret them.

The sequence of horizontal EW pulses during the Northridge earthquake, which had maximum amplitudes less than 12 cm (Figure 3a) caused severe damage but did not cause collapse. In order to simulate collapsing stages of the model, the amplitudes of the horizontal pulses were amplified 14 times [1]. After this magnification, the amplitudes of the consecutive horizontal pulses are $A = 154, 168, 140, 112$, and 98 cm, and their durations are $t_d = 1.8, 1.4, 2.3, 1.5$, and 2.4 s. The horizontal pulses are combined with vertical pulses to have amplitudes A, which are 1/5, 1/2, and 3/4 of those of the corresponding horizontal pulses and durations t_d, which are the same as those of the horizontal pulses. The vertical pulses are all upward or all downward. These pulse amplitudes and durations are not specific to a particular earthquake but are expected to be similar to those found in the vicinity of faults breaking the ground surface.

We select the vertical pulses to have amplitudes equal to 1/5, 1/2, and 3/4 of the amplitudes of the horizontal pulses to illustrate the consequences of incident wave motion arriving at the building site with different incident angles. In this paper, we illustrate the response only for the pulses that can be thought of as representing body waves. We will investigate how the surface Love and Rayleigh waves contribute to the collapsing of buildings in our future papers.

In our previous study [1], we subjected the same building model to the same sequence of five horizontal pulses and observed that the collapse occurred at the end of the fifth pulse. For pulses with larger amplitudes, collapse would occur sooner, which can be shown with a more detailed analysis. In the following examples, the model is excited by simultaneous horizontal and vertical pulses and will experience progressively increasing permanent strains, which will bring it sooner to collapse.

Figures 6–9 present selected results. In all of them, the plots in the first row show the displacements along the building height at different time instances. The red lines on the top mark the ±1% and ±10% drift amplitudes, corresponding to the displacement scale at the bottom. The different lines correspond to a sequence of the building model positions eventually leading to collapse. The center row shows the pulses and the times when the collapse is initiated and completed. The bottom row shows the vertical and horizontal positions of the top of the building up to the time of collapse. The plots in the second row show the corresponding input displacement pulses. The third row of plots (in Figures 8 and 9 only) shows the horizontal and vertical displacement of the roof at the time of collapse.
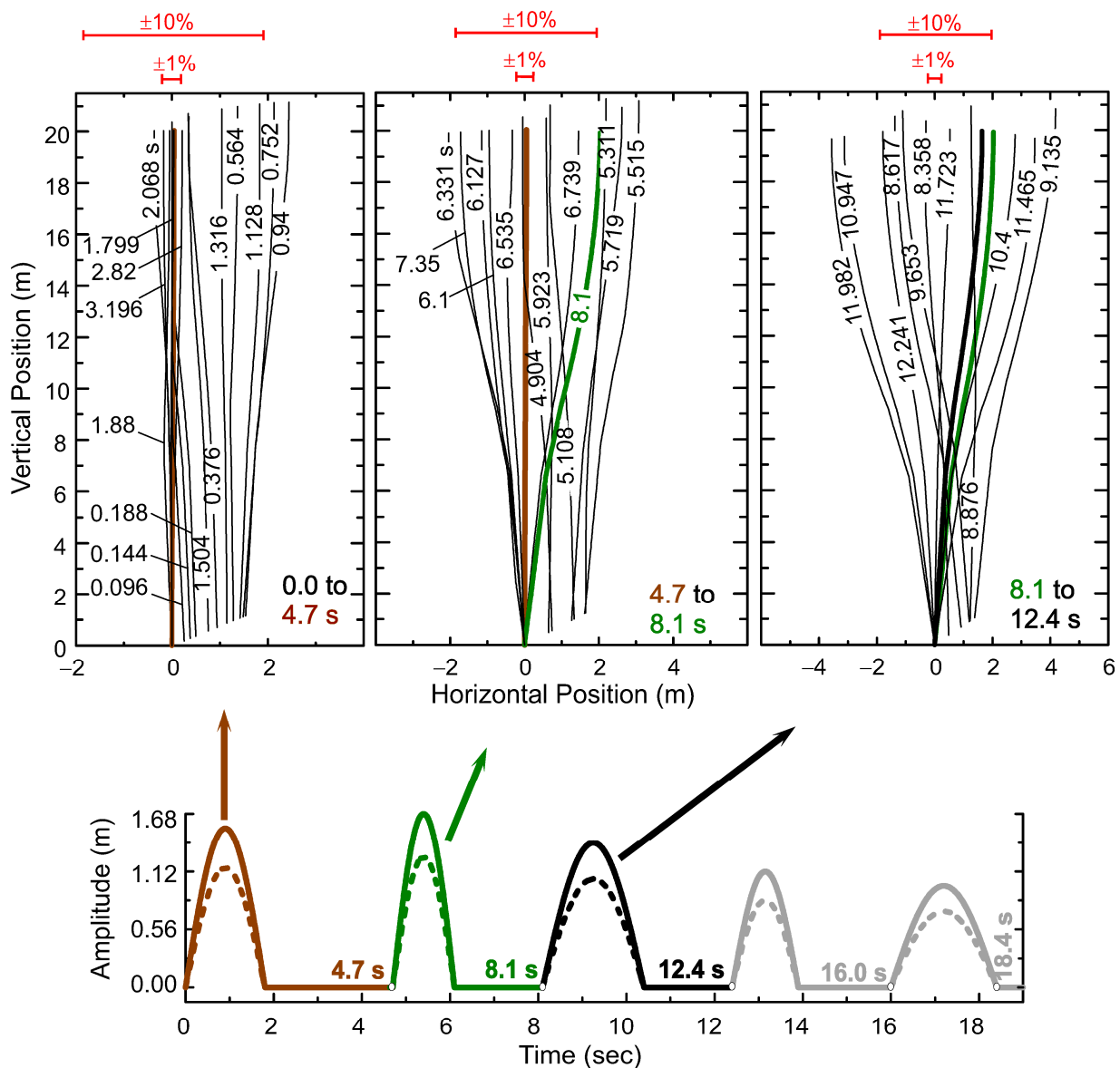

Figure 6. (Top) Plots of the model displacement during the excitation by each one of the first three pulses. During and after the first pulse, the interstory drift exceeded 10%. The roof displacements that correspond to the interstory drift of 1% and 10% are indicated by red lines on the top of the plots. The different lines show the displacements at different time instances. The heavy lines indicate the start and end time of the corresponding time interval. (Bottom) The input horizontal (solid lines) and upward vertical (dashed lines) pulses. In this example, the vertical pulses have amplitudes that are 3/4 of those of the corresponding horizontal pulses.
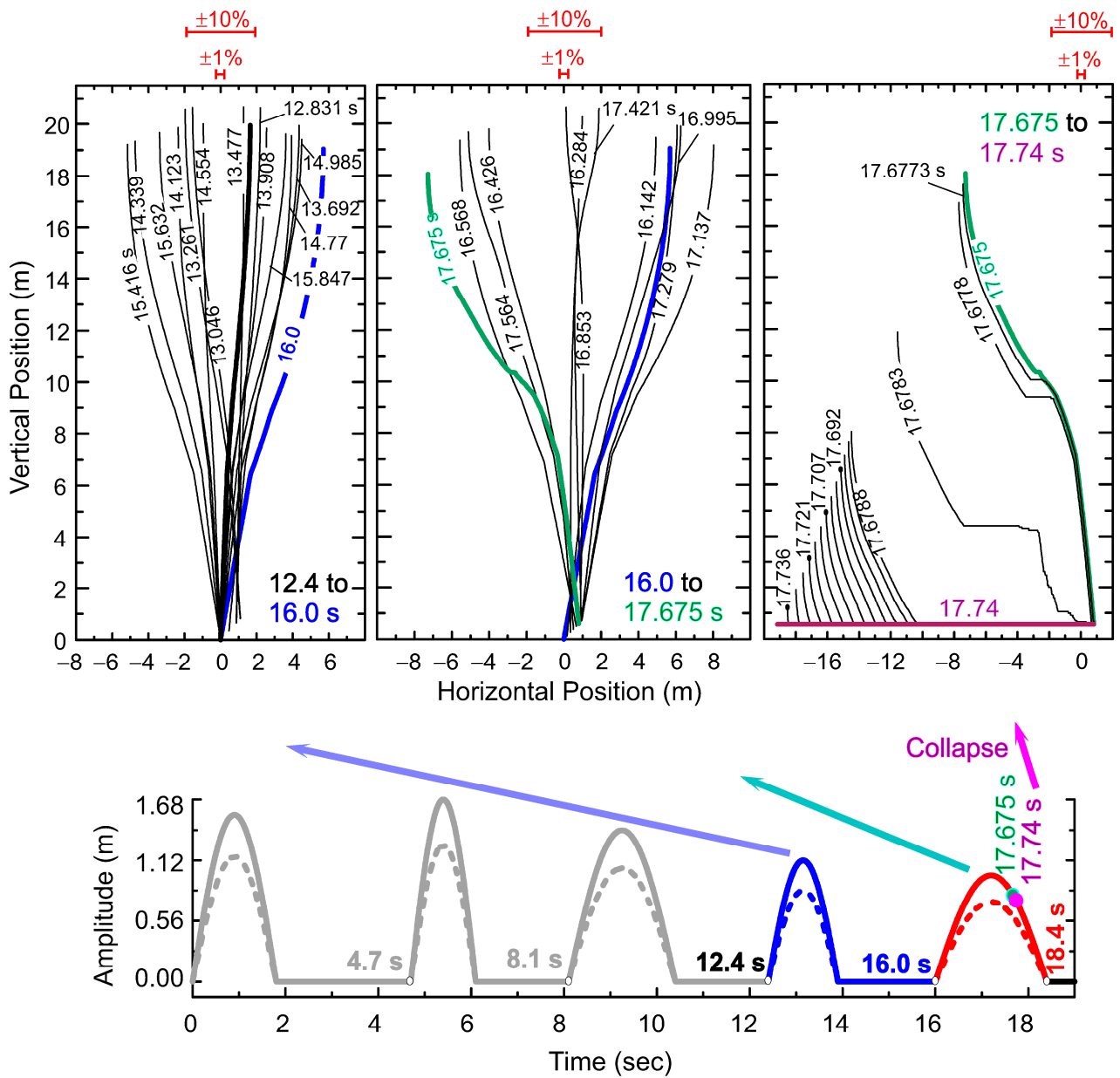
Figure 7. Same as Figure 6 but showing the model displacement during excitation by the fourth and fifth pulses. Collapse begins at 17.765 s and is completed at 17.74 s.
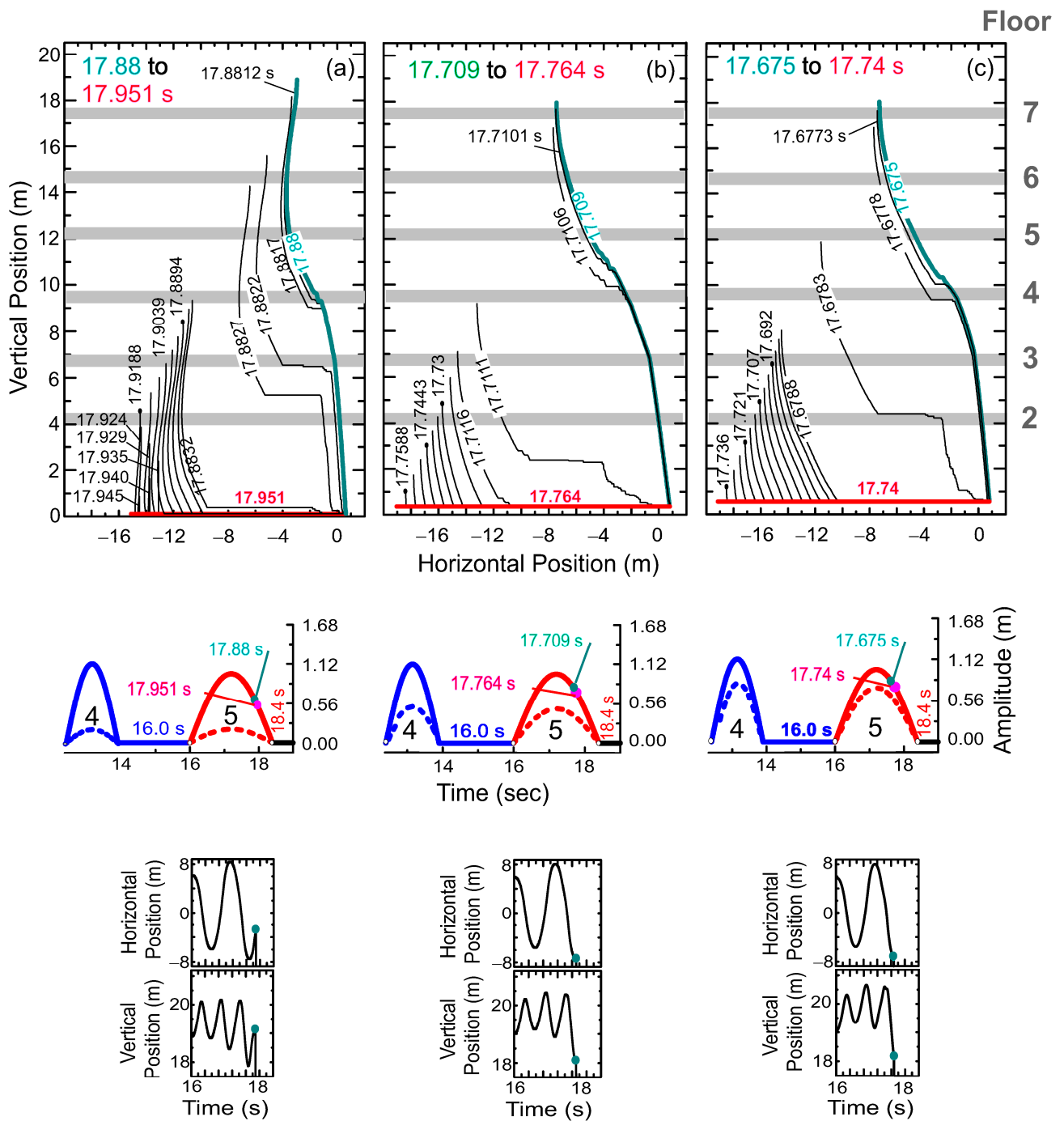
Figure 8. (Top) The model displacement during the collapsing stages of the structure for different amplitudes of the *upward* vertical pulses: 1/5 (part (**a**)), 1/2 (part (**b**)), and 3/4 (part (**c**)) of those of the horizontal pulses. The horizontal wide gray lines mark building floors 2 through 7. (Middle) The last two of the sequence of five pulses during which collapse occurs. (Bottom) Horizontal and vertical positions of the roof of the building model around the time of collapse. The green dot indicates the start of collapse.
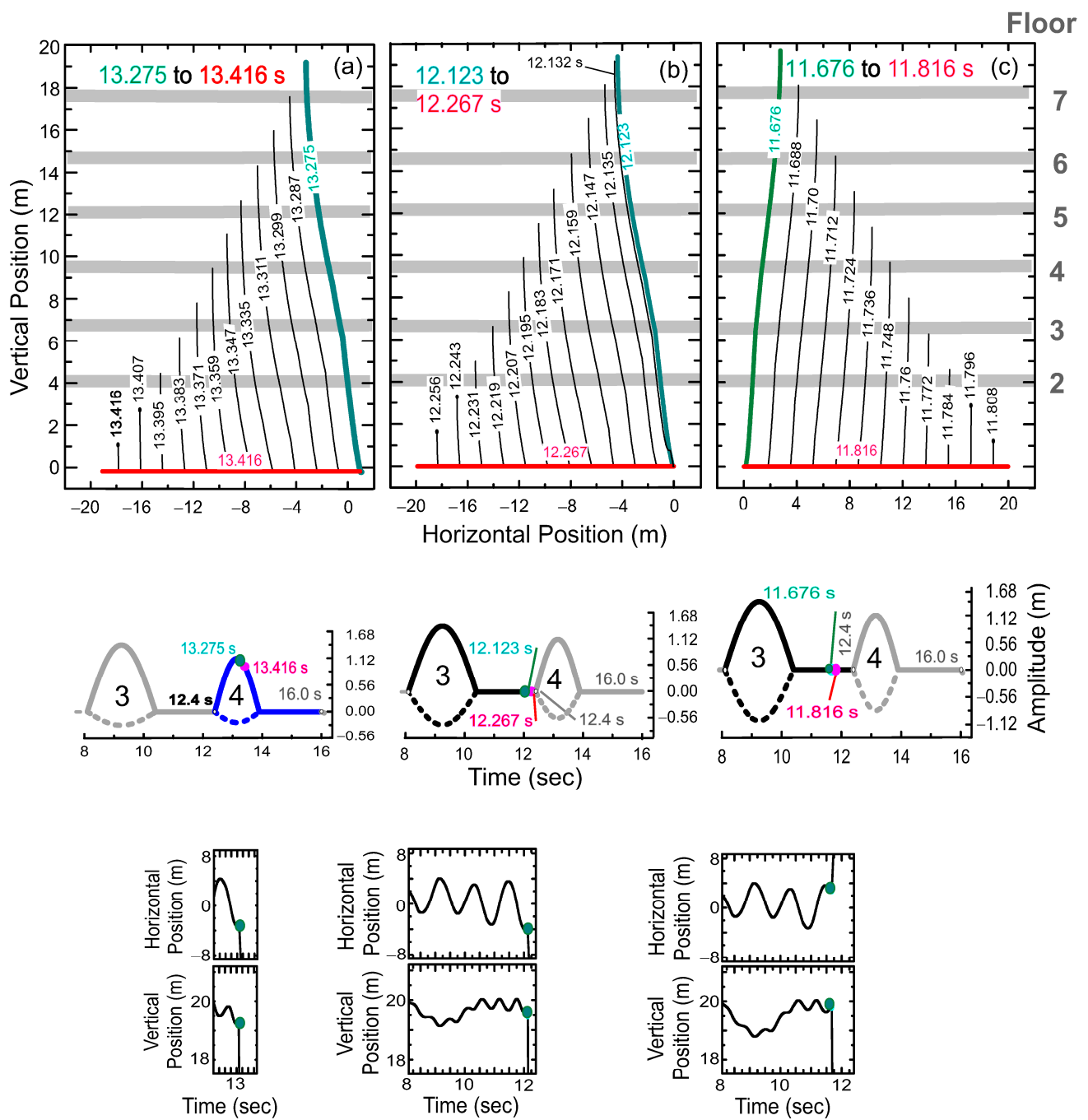
Figure 9. Same as Figure 8, but for *downward* vertical pulses. In this example, collapse occurs during the third and fourth pulses.

In the examples shown in Figures 6 and 7, the vertical pulses act upward and have amplitudes equal to 3/4 of those of the horizontal pulses. Figure 6 shows the displacements during excitation by the first three pulses. During the first pulse, the drift amplitudes already exceed 10%, and during the response to the second and third pulses, the drifts become significantly larger than 10%. These are large displacements that exceed the threshold of tolerable drift amplitudes [36]. Although the building is severely damaged, it is still standing. Figure 7 shows the displacements during excitation by the last two pulses. During the action of the last two pulses, between 12.4 s and 17.675 s, the displacements still oscillate, but are progressively larger, corresponding to and exceeding 20% drift. Then,

between 17.675 s and 17.74 s, the gravity forces the building to rapidly fall. The collapse occurs at 17.74 s.

Figures 8 and 9 show the last stages of collapse, respectively for vertical pulses acting upward and downward. Each of these two figures has three columns ((a) to ((c)), which correspond to different scaling factors of the amplitudes of the vertical pulses (1/5, 1/2, and 3/4). The plots show only the pulses during which collapse occurs (pulses 4 and 5 in Figure 8 and pulses 3 and 4 in Figure 9). It is seen that, in all cases, the final stage of the collapse begins when the horizontal displacements of the top of the building are large, and the top of the building oscillates with a period of 1.054 s. The oscillation in the vertical position of the top of the building has period 0.527 s and results from up and down movements of the top associated with its horizontal motion.

The location where collapse begins is different in Figures 8 and 9. In the former, the final stage of the collapse starts near mid-height, and then progresses due to the action of gravity. In all three cases shown in Figure 8, the building collapses to the left. In Figure 9, the collapse begins at the base of the building, and then progresses up toward the other elements. In this figure, the building collapses to the left in cases (a) and (b), and toward the right in case (c).

In Figure 8, the vertical ground pulses act upward, thus increasing the axial forces in the structural members carrying the vertical loads in buildings modeled by our simplified shear beam. This moves the axial loads in the columns closer to their critical buckling loads. In Figure 9, the vertical ground pulses act downward, thus decreasing the axial loads in the columns due to the gravity loads. It is seen that, for very large ground motions in the vicinity of faults with very large dislocation amplitudes, this can lead to short time intervals during which the compression forces in the columns due to the weight of the building can become negative (tension). We will investigate the consequences of these increases and decreases of forces in columns for different construction materials (concrete, steel, wood, masonry, etc.) in our future studies.

4. Discussion and Conclusions

We described the collapsing stage of a nonlinear model of a shear building subjected to large amplitude horizontal and vertical displacement pulses at its base, including the effects of gravity. The duration of these pulses was chosen to be similar to the ground motion recorded at a building site (Figure 3a) in the central San Fernando Valley during the 1994 earthquake in Northridge, California, but the amplitudes of the horizontal pulses were magnified 14 times and those of the vertical pulses were magnified by factors of 2.8, 7, and 10.5 to provide a collapse condition. It was shown that, for the example considered, for downward vertical pulses, the collapse began at the first element (counted from the base upward), and then extended to the elements above it. For upward vertical pulses, the collapse was initiated at the elements at mid-height. The collapse was initiated sooner in the case of downward vertical pulses as compared to the case of upward vertical pulses.

The shear-beam model, selected for this analysis, is based on the assumption that the building columns are infinitely rigid under the action of the axial forces, and thus do not deform. Therefore, considering M–N (moment–axial force) interaction and its role in analyzing the collapse of this building's columns does not come into play. The collapsing mechanism in this building model can be viewed as occurring due to the creation of plastic hinges at the top and bottom of the columns, which eventually allows the columns to collapse toward the horizontal (collapsed) direction, equal to $\pm\pi/2$.

Many current methods for analyzing the structural response in the collapse phase require sudden removal of one or more main structural members to initiate failure. In contrast, the model presented in this paper does not require this starting point. The presented model naturally begins to experience large strains and dynamic instability when the wave motion in the structure creates large nonlinear deformations and an unbalanced configuration. The generalization of this model will be valuable for the analysis of structural response and failure mechanisms during other extreme events that are associated with very

large loads (high winds, heavy debris carried by tsunami inundation, projectile loading and penetration, above-and-within ground explosions, collisions with heavy objects, and many others).

Author Contributions: Conceptualization, M.D.T.; methodology H.A., V.G., M.D.T. and R.S.J.; software, H.A. and V.G.; validation, H.A., V.G. and M.D.T.; formal analysis, H.A., V.G., M.D.T. and R.S.J.; investigation, H.A., V.G., M.D.T. and R.S.J.; writing—original draft preparation, H.A., M.D.T. and R.S.J.; writing—review and editing, M.I.T.; visualization, H.A., M.D.T. and M.I.T. All authors have read and agreed to the published version of the manuscript.

Data Availability Statement: No data were used in this study. All results presented have been generated using computer codes developed by the authors.

Conflicts of Interest: The authors declare no conflict of interest.

References

1. Abbasgholiha, H.; Gičev, V.; Trifunac, M.; Jalali, R.; Todorovska, M.I. Collapsing response of a nonlinear shear-beam building model excited by a strong-motion pulse at its base. *Geohazards* **2023**, *4*, 40–62. [CrossRef]
2. Adam, J.M.; Parisi, F.; Sagaseta, J.; Li, X. Research and practice on progressive collapse and robustness of building structures in the 21st century. *Eng. Struct.* **2018**, *173*, 122–149. [CrossRef]
3. El-Towil, S.; Li, H.; Kunnath, S. Computational simulation of gravity-induced progressive collapse of steel frame buildings: Current trends and future needs. *J. Struct. Eng.* **2014**, *140*, 1–12. [CrossRef]
4. Byfeld, M.; Mudalige, W.; Morison, C.; Stoddart, C. A review of progressive collapse research and regulation. *Proc. Inst. Civ. Eng. Struct. Build.* **2014**, *167*, 447–466. [CrossRef]
5. Qian, K.; Li, B. Research advances in design of structures to resist progressive collapse. *J. Perform. Construct. Fac.* **2015**, *29*, 1–11. [CrossRef]
6. Kunnath, S.K.; Bao, Y.; El-Tawil, S. Advances in computational simulation of gravity-induced disproportionate collapse of RC frame buildings. *J. Struct. Eng.* **2018**, *144*, 1–18. [CrossRef]
7. Sharafi, P.; Alembagheri, M.; Kildashti, K.; Ganji, H.T. Gravity-induced progressive collapse response of precast corner-supported modular buildings. *J. Archit. Eng. ASCE* **2021**, *27*, 04021031. [CrossRef]
8. Thai, H.-T.; Ho, Q.V.; Li, W.; Ngo, T. Progressive collapse and robustness of modular high-rise buildings. *Struct. Infrastruct. Eng.* **2021**, *19*, 302–314. [CrossRef]
9. Alembagheri, M.; Sharafi, P.; Hajireazei, R.; Tao, Z. Anti-collapse resistance mechanisms in corner-supported modular steel buildings. *J. Constr. Steel Res.* **2020**, *170*, 106083. [CrossRef]
10. Hadi, M.N.S. New building scheme to resist progressive collapse. *J. Archit. Eng. ASCE* **2012**, *18*, 324–331. [CrossRef]
11. Manie, S.; Moghadam, A.S.; Ghafory-Ashtiany, M. Collapse behavior evaluation of asymmetric buildings subjected to bi-directional ground motion. *Struct. Des. Tall Spec. Build.* **2015**, *24*, 607–628. [CrossRef]
12. Song, B.; Sezen, H. Experimental and analytical progressive collapse assessment of steel frame building. *Eng. Struct.* **2013**, *56*, 664–672. [CrossRef]
13. Fang, C.; Linzell, D. Examining progressive collapse robustness of a high-rise reinforced concrete building. *Eng. Struct.* **2021**, *248*, 113274. [CrossRef]
14. Gičev, V.; Trifunac, M.D. Permanent deformations and strains in a shear building excited by a strong motion pulse. *Soil Dyn. Earthq. Eng.* **2007**, *27*, 774–792. [CrossRef]
15. Gičev, V.; Trifunac, M.D. Transient and permanent rotations in a shear layer excited by strong earthquake pulses. *Bull. Seism. Soc. Am.* **2009**, *99*, 1391–1403. [CrossRef]
16. Gičev, V.; Trifunac, M.D. Transient and permanent shear strains in a building excited by strong earthquake pulses. *Soil Dyn. Earthq. Eng.* **2009**, *29*, 1358–1366.
17. Trifunac, M.D. 75th anniversary of strong motion observation—A historical review. *Soil Dyn. Earthq. Eng.* **2009**, *29*, 591–606.
18. Murphy, L.M. *San Fernando, California, Earthquake of February 9, 1971*; Murphy, L.M., Ed.; U.S. Department of Commerce, National Oceanic and Atmospheric Administration: Washington, DC, USA, 1973.
19. Trifunac, M.D.; Ivanović, S.S.; Todorovska, M.I. *Instrumented 7-Storey Reinforced Concrete Building in Van Nuys, California: Description of Damage from the 1994 Northridge Earthquake and Strong Motion Data*; Report CE 99-02; University of Southern California: Los Angeles, CA, USA, 1999.
20. Trifunac, M.; Hao, T.Y. *7-Storey Reinforced Concrete Building in Van Nuys, California: Photographs of the Damage from the 1994 Northridge Earthquake*; Report CE 01-05; University of Southern California: Los Angeles, CA, USA, 2001.
21. Islam, M.S. *Analysis of the Response of an Instrumented 7-Story Non Ductile Concrete Frame Building Damaged during the Northridge Earthquake*; 1996 Annual Meeting, Professional Paper 96-9; Los Angeles Tall Buildings Structural Design Council: Los Angeles, CA, USA, 1996.

22. Li, Y.R.; Jirsa, J.O. Nonlinear analyses of an instrumented structure damaged in the 1994 Northridge earthquake. *Earthq. Spectra* **1998**, *14*, 265–283. [CrossRef]

23. Ivanović, S.S.; Trifunac, M.D.; Novikova, E.I.; Gladkov, A.A.; Todorovska, M.I. *Instrumented 7-Storey Reinforced Concrete Building in Van Nuys, California: Ambient Vibration Surveys following the Damage from the 1994 Northridge Earthquake*; Report CE 99-03; University of Southern California: Los Angeles, CA, USA, 1999.

24. Trifunac, M.D.; Ivanović, S.S.; Todorovska, M.I.; Novikova, E.I.; Gladkov, A.A. Experimental evidence for flexibility of a building foundation supported by concrete friction piles. *Soil Dyn. Earthq. Eng.* **1999**, *18*, 169–187. [CrossRef]

25. Ivanović, S.S.; Trifunac, M.D.; Novikova, E.I.; Gladkov, A.A.; Todorovska, M.I. Ambient vibration tests of a seven-story reinforced concrete building in Van Nuys, California, damaged by the 1994 Northridge Earthquake. *Soil Dyn. Earthq. Eng.* **2000**, *19*, 391–411. [CrossRef]

26. Browning, J.A.; Li, R.Y.; Lynn, A.; Moehle, J.P. Performance assessment for a reinforced concrete frame building. *Earthq. Spectra* **2000**, *16*, 541–555. [CrossRef]

27. De la Llera, J.C.; Chopra, A.K.; Almazan, J.L. Three-dimensional inelastic response of an RC building during the Northridge earthquake. *J. Struct. Eng. ASCE* **2001**, *127*, 482–489. [CrossRef]

28. Ivanović, S.S.; Trifunac, M.D.; Todorovska, M.I. On identification of damage in structures via wave travel times. In Proceedings of the NATO Advanced Research Workshop on Strong-Motion Instrumentation for Civil Engineering Structures, Istanbul, Turkey, 2–5 June 1999; Kluwer Academic Publishers: Dordrecht, The Netherlands, 2001; pp. 447–468.

29. Trifunac, M.D.; Ivanović, S.S. *Analysis of Drifts in a Seven-Story Reinforced Concrete Structure*; Report No. CE 03-01; University of Southern California: Los Angeles, CA, USA, 2003.

30. Todorovska, M.I.; Trifunac, M.D. Impulse response analysis of the Van Nuys 7-story hotel during 11 earthquakes and earthquake damage detection. *Struct. Control Health Monit.* **2008**, *15*, 90–116. [CrossRef]

31. Gičev, V.; Trifunac, M.D. A note on predetermined earthquake damage scenarios for structural health monitoring. *Struct. Control Health Monit.* **2012**, *19*, 746–757. [CrossRef]

32. Shakal, A.; Huang, M.; Darragh, R.; Cao, T.; Sherburne, R.; Malhotra, P.; Cramer, C.; Syndov, R.; Graizer, V.; Maldonado, G.; et al. *CSMIP Strong-Motion Records from the Northridge, California, Earthquake of 17 January 1994*; Report No. OSMS 94-07; California Department of Conservation, Division of Mines and Geology: Sacramento, CA, USA, 1994.

33. Trifunac, M.D. A three-dimensional dislocation model for the San Fernando, California, earthquake of February 9, 1971. *Bull. Seism. Soc. Am.* **1974**, *64*, 149–172. [CrossRef]

34. Wald, D.J.; Heaton, T.H. The slip history of the 1994 Northridge, California, earthquake determined from strong-motion, teleseismic, GPS and leveling data. *Bull Seism. Soc. Am.* **1996**, *86*, S49–S70. [CrossRef]

35. Lax, P.D.; Wendroff, B. Difference schemes for hyperbolic equations with high order of accuracy. *Commun. Pure Appl. Math.* **1964**, *XVII*, 381–398. [CrossRef]

36. Ghobarah, A. On drift limits associated with different damage levels. In Proceedings of the International Workshop on Performance-Based Seismic Design, Bled, Slovenia, 28 June–1 July 2004; pp. 321–332.